Polarized spectral emittance from periodic micromachined surfaces. II. Doped silicon: Angular variation

Peter J. Hesketh* and Jay N. Zemel
Department of Electrical Engineering and Center for Sensor Technologies, University of Pennsylvania, Philadelphia, Pennsylvania 19104-6390

Benjamin Gebhart
Department of Mechanical Engineering and Applied Mechanics, University of Pennsylvania, Philadelphia, Pennsylvania 19104-6390

(Received 27 February 1987; revised manuscript received 16 February 1988)

The polarized directional spectral ($3\ \mu m \leq \lambda \leq 14\ \mu m$) emittances (PDSE's) of highly doped, micromachined, periodic structures on silicon were measured. These structures have dimensions that are comparable to the wavelengths of the measured radiation. Significant anisotropies and maxima were found for the *s* and *p* PDSE's measured in emittance planes parallel and perpendicular to the grating-repeat vector. Wood's singularities were clearly visible in the *p* PDSE on shallow gratings (depth $\leq 1.5\ \mu m$). Periodic maxima were observed in both the *s* and *p* PDSE in the emittance plane perpendicular to the grating vector due to standing-wave modes in the slots of the grating. It is concluded that the PDSE provides detailed information on the characteristics of the electromagnetic modes associated with surface microstructures.

I. INTRODUCTION

Recently, the authors demonstrated maxima in the normal polarized spectral emission from highly doped, micromachined [microconfigured (MC)] silicon surfaces that were periodic in wave number.[1] This behavior arises from electromagnetic standing waves, analogous to organ-pipe modes, in deep-grating slots. This model for the normal polarized spectral emittance of MC surfaces was examined further in the preceding paper,[2] hereafter referred to as I. In this paper, measurements are reported of polarized directional spectral emittance (PDSE) from the same set of samples as those in I and the results are interpreted with the standing-wave model.

As is well known, thermal radiative emissions from a solid arise from the thermal motion of charges in the solid.[3-5] The emissivity of a metal is smaller than that of a dielectric because of partially screening of the electromagnetic field by the mobile charge carriers in the metal. The PSDE, $\varepsilon(\theta,\phi,\lambda,p_i,T)$, is equal to the polarized directional spectral absorptance by Kirchoff's law. Here θ is the polar angle measured with respect to the normal in the emittance plane of the MC surface, ϕ is the azimuthal angle measured in the surface plane with respect to the perpendicular to the primary propagation vector Λ of the periodic component of the MC geometry, p_i is the polarization of the emitted radiation (of wavelength λ) relative to the emittance plane (see Fig. 1) and T is the sample temperature. For all the measurements presented in this paper, $T = 400\,^{\circ}C$. As shown in Fig. 1, the *s* polarization is perpendicular to the emission plane and the *p* polarization is parallel to it. In this figure the emission plane is shown at an arbitrary azimuthal angle ϕ. The results to be presented in this paper were taken for the two high-symmetry directions of $\phi = 0°$ and 90°. The results obtained for $\phi = 0°$ are new to the best of our knowledge.

If the emission arises from a flat and homogeneous surface on a semi-infinite solid, then[5]

$$e(\theta,\phi,\lambda,p_i) = 1 - r(\theta,\phi,n(\lambda),k(\lambda),p_i)\ ; \quad (1)$$

where $r(\theta,\phi,n(\lambda,k(\lambda),p_i)$ is the reflectivity of the sur-

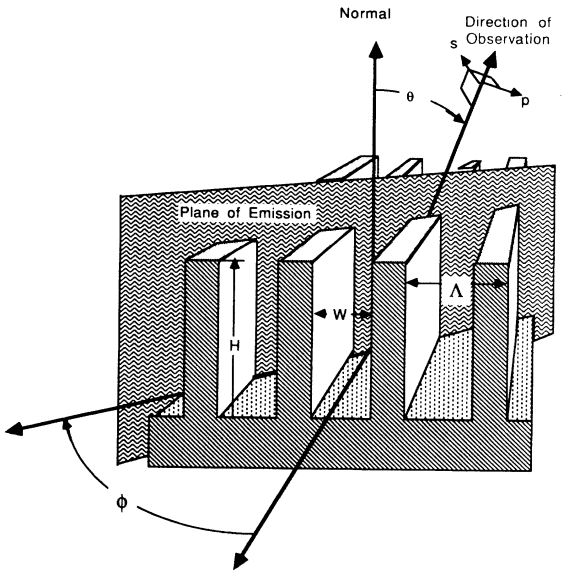

FIG. 1. Coordinate system for the polarized, directional, spectral emittance. Λ is the grating propagation vector, H is the depth of the grating slot, W is the width of the slot, θ is the polar angle measured relative to the normal to the microconfigured surface, and ϕ is the azimuthal angle. The *p* polarization lies in the plane of emission and the *s* polarization is perpendicular to that plane. Not shown is the length of the slots, L.

face. $r(\theta,\phi,n(\lambda),k(\lambda),p_i)$ can be expressed in terms of the spectral index of refraction $n(\lambda)$, the spectral extinction coefficients $k(\lambda)$, and the Fresnel coefficients.[3,6,7] As is well known, the Fresnel coefficients are independent of ϕ for an isotropic material such as silicon. As a result, it can be shown that the reflectivity for s and p polarizations are the same. $n(\lambda)$ and $k(\lambda)$ are related to the real and imaginary parts of the dielectric constant (assuming homogeneity and isotropy) by the well-known expressions

$$\epsilon_1(\lambda)=n^2(\lambda)-k^2(\lambda)\ , \tag{2a}$$

$$\epsilon_2(\lambda)=2n(\lambda)k(\lambda)\ . \tag{2b}$$

In its simplest version, $\epsilon_1(\lambda)$ and $\epsilon_2(\lambda)$ can be calculated from the Drude model.[4] This leads to the well-known expressions

$$\epsilon_1=\epsilon_\infty\left[1-\frac{\omega_p^2}{\omega^2+1/\tau^2}\right]\ , \tag{3a}$$

$$\epsilon_2=\frac{\epsilon_\infty\omega_p^2}{\omega\tau(\omega^2+1/\tau^2)}\ , \tag{3b}$$

where ϵ_∞ is the high-frequency dielectric constant and τ is the optical relaxation time. ω_p is the plasma frequency

$$\omega_p^2=\frac{Nq^2}{m_0m^*\epsilon_0\epsilon_\infty}\ , \tag{4}$$

where m_0 is the free electron mass, m^* is the effective mass, N is the number of free carriers, ω is the radial frequency $2\pi c/\lambda$, and q is the electronic charge. The angular dependence of the reflectivity can be readily obtained from these relations and when combined with Eq. (1), the PDSE is easily obtained for a flat surface in terms of the number of carriers, their effective mass and relaxation time. This free-carrier absorption theory (FCA) has not been applied to the directional emissivity of heavily doped silicon to the best of our knowledge. The only published information deals with the calculated emittance from absorptance studies and measurements of the normal emittance.[7]

No other PDSE studies have been found dealing with periodic microconfigured surfaces. However, there has been considerable interest in anomalous absorption on diffraction gratings ever since the original study by Wood in 1902.[8] This phenomenon has been studied on shallow gratings with aspect ratios less than unity. The aspect ratio is the gratings depth H, divided by the grating repeat distance Λ. Wood and subsequent investigators observed that when p-polarized electromagnetic waves interact with a diffraction grating oriented at $\phi=90°$, a rapid variation is seen in the reflectance spectrum. Wood terms these as "singular anomalies." These variations, associated with resonant absorption processes on the grating at the onset or disappearance of particular spectral diffraction orders, are known as Rayleigh wavelengths λ_R, which depend on θ and Λ as

$$\lambda_R=\frac{\Lambda}{m}(\sin\theta\pm1)\ , \tag{5}$$

where m is an integer. The studies with diffraction gratings having depths greater than the incident wavelength produced singularities in the s-polarized light which were not predicted by the earlier theories based on $\lambda>H$.[9] Hessel and Oliner showed theoretically that[10] (a) the polar-angle dependence of the absorptance varied rapidly for the p polarization and (b) the absorption maximum, in both s and p polarization, suggests a resonant behavior dependent on the grating depth which disappears when $H\leq\lambda$. These two effects were demonstrated by representing the grating as an equivalent surface impedance structure. Both effects occur close to the Rayleigh wavelengths and at an angle of $\phi=90°$. The type (a) p-polarized singularities are due to the launching of a surface electromagnetic wave or surface plasmon of wavelength, λ_{SP}. This results in an additional mechanism for loss, thus increasing the absorption. The surface-plasmon wave vector, $k_{SP}=2\pi/\lambda_{SP}$, is given by[11]

$$k_{SP}=\frac{\omega}{c}\left[\frac{\epsilon_1(\lambda)}{1+\epsilon_1(\lambda)}\right]^{1/2}\ . \tag{6}$$

The surface plasmon may only exist for the wavelength regime between the bulk plasmon λ_{BP}, and where $\epsilon_1(\lambda)=0$. For silicon in the wavelength range corresponding to our measurements, $\epsilon_1(\lambda)<0$. Thus the lower bound is $\lambda=\lambda_{BP}$. For the absorption of the incident wave vector $\mathbf{k}$ by a surface plasmon, the component that parallels the surface couples to the surface plasmon through the grating "effective" wave vector, $2\pi/\Lambda$, yielding[12]

$$\sin\theta=\left[\frac{\epsilon_1(\lambda)}{1+\epsilon_1(\lambda)}\right]-\frac{m\lambda}{\Lambda}\ . \tag{7}$$

This equation will be used in interpreting the directional spectral p-polarized emittance data at $\phi=90°$ in Sec. III A. The type (b) singularities have been demonstrated both theoretically and experimentally and are observed at the Rayleigh wavelengths. Absorption singularities, in close agreement with theory, have also been found in the microwave region on shallow gratings[13,14] and in the infrared.[15] Similar behavior would be expected in the emission characteristics, but have not been observed until now. The p-polarized absorptance maxima or Wood's singularity can give rise to total absorption at a shallow grating.[16] Total absorption of s-polarized light has been observed for a dielectric coated metallic grating.[17]

Other experimental and theoretical studies have considered the effect of a dielectric layer on the grating.[12] One study demonstrated that a $\lambda/5$ thick dielectric layer produced a splitting of the p-polarized maxima and a pronounced enhancement of the strength of the s-polarized singularity.[18] The influence of surface coatings on MC emission will not be considered in this paper. Measurements of the directional spectral polarized absorptance of silvered gratings and calculations by Glass and Maradudin have been discussed in I.

Surface roughness of various types has a strong effect on the directional emittance. Several studies have shown that the measured directional emittance on randomly rough surfaces increases with polar angle, but less rapidly than for smooth surfaces. The directional emittance also appears to be independent of azimuthal angle. Rolling

observed an overall increase for rough platinum surfaces, with more energy concentrated in the normal direction ($\theta=0°$).[19] In addition, when the directional emittance at 1.5 and 6 μm are compared, surface roughness has a greater effect at the longer wavelength. Calculations and measurements of emittance, based on geometric optics and a Gaussian distribution of asperity heights, are in reasonable agreement with observations. Agreement is best at small polar angles, where shadowing of adjacent protrusions does not occur. Also, agreement is closest for wavelengths much smaller than the rms roughness. This model is not applicable to the regular microstructures examined here. Demont *et al.* studied the emittance of *v*-shaped and other groove geometries, conical, cylindrical, and hemispherically shaped cavities both experimentally and theoretically.[20] In some cases, strongly directional properties were observed. Calculations based on a geometric optics model are in close agreement with the data. These results are the small wavelength, asymptotic limit to the work reported here. However, they provide a standard of comparison for the data when the scale of the roughness is much greater than the wavelength. This has been reported elsewhere.[21]

II. EXPERIMENTAL PROCEDURES

The preparation, general description of the samples, and an outline of the experimental methods used in the PDSE studies are given in I. To carry out the angular dependent emittance measurements, a stepping motor driven goniometer was constructed. The sample is mounted on a thermally insulated substrate on the goniometer. The goniometer stepping motor produces rotation of the polar angle θ from 0° to 75°. The azimuthal angle ϕ was manually adjusted from 0° to 180°. The stepping motor operated under digital control from the microcomputer. The resolution, limited by a single step of the motor, is 0.9°. The polar angle increments actually employed in the measurements was 5°. This relatively coarse angular increment was dictated by the 5° angular diameter of the spectrometer system condensing mirror that focused the energy from the MC surface on the spectrometer entrance slit as indicated in Fig. 3 of I. The azimuthal adjustment was carried out manually with a graticule accuracy of 2°.

The observed surface area of the radiating sample subtended by the entrance slit of the spectrometer was 0.5×5.0 mm^2 at $\theta=0°$. As the substrate was rotated, the radiating surface area imaged by the entrance aperture of the spectrometer increased as secθ. The maximum θ was limited by the width of the sample. Because a region of uniform temperature was required, a more stringent limit was imposed so that only half the available length, that is 6 mm, was imaged onto the entrance aperture. This yielded a maximum angle of 85° for θ. Since the entrance slit of the spectrometer is curved, the maximum polar angle had to be further restricted to a value of 75°. As in I, the sample was uniformly heated by the integrated heater on the back of the sample. Typically, 4 W of power was dissipated.

The directional spectral emittance was measured in two stages for each particular wavelength. The sample was moved to the focal point of the spectrometer and aligned. Then the background emission from the spectrometer, $I_{a,n}(\lambda,p_i,T_0)$ was measured and stored in the data logger. T_0 is the background temperature of the spectrometer. The radiant flux, $I_S(\theta,\phi,\lambda,p_i,T)$, from the sample was measured at a temperature T as a function of θ and stored. Following this, the normal polarized spectral emittance from the blackbody source was measured and stored. The normalized sample emittance was then calculated as follows:

$$\frac{e(\theta,\phi,\lambda,p_i,T)}{e(0,\phi,\lambda,p_i,T)}=\frac{(I_{S,\lambda}(\theta,\phi,\lambda,p_i,T)-I_{a,n}(\lambda,p_i,T_0))}{(I_{S,\lambda}(0\Upsilon,\phi,\lambda,p_i,T)-I_{a,n}(\lambda,p_i,T_0))}\ . \tag{8}$$

The absolute directional spectral emittance was calculated by multiplying $e(\lambda,\theta,\phi,p_i,T)$ by the normal polarized spectral emissivity [Eq. (1) of I].

III. EXPERIMENTAL RESULTS AND DISCUSSION

The PDSE for a smooth, heavily doped silicon surface is presented initially. These results are then analyzed using the FCA theory outlined in Sec. I. Following this, the extensive experimental PDSE data taken on specimens with four different repeat distances, $\Lambda=10$, 14, 18, and 22 μm, are presented. It should be noted that MC surfaces have a high degree of symmetry corresponding to the direction of the grating vector(s). As a result, we chose to examine the emission along planes corresponding to the two different high-symmetry azimuthal angles, $\phi=0°$ and 90° and for the two polarizations. The presentation of the information has been organized to reflect these symmetries. The PDSE polar angular range is $0°\le\theta\le75°$ for all of the data shown. The samples used in the PDSE study are the same as those used in I. Only data which show the most pertinent features of the phenomena observed have been selected for inclusion here.

A. Smooth silicon

The PDSE of heavily doped silicon has not been reported in the literature. In Fig. 2 the measured values of PDSE are plotted as a solid line for selected wavelengths in the range $3\ \mu\text{m}\le\lambda<14\ \mu$m. As expected for a metallic surface, the *s*-polarized emission decreases monotonically with polar angle, Fig. 2(a), and the *p*-polarized emission increases, Fig. 2(b). The *s* electric field is more effectively screened as the polar angle increases and $e(\theta,\phi,s,400\,°\text{C})$ decreases monotonically in magnitude. The *p* electric field may be split into two components, one perpendicular and the other parallel to the surface. The parallel component is in the same direction as the *s*-polarized electric field. The perpendicular component is less effectively screened as θ increases. Therefore, $e(\theta,\phi,p,400\,°\text{C})$ may reach a maximum value at some polar angle. For a perfect conductor, the maximum would occur at approaching $\theta=90°$. Note that the slope of the curve at large θ increases as λ increases. This indicates that the surface at this wavelength is behaving in a more metallic fashion.

The PDSE was calculated using FCA theory [Eqs.

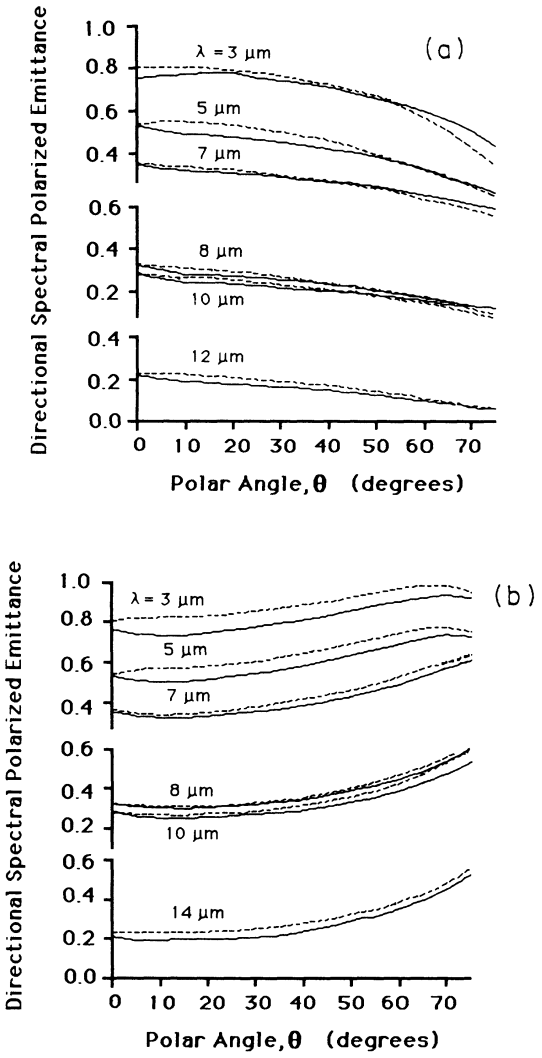

FIG. 2. Polarized directional spectral emissivity of 1.6×10^{20} cm^{-3} phosphorus-doped smooth silicon at 400 °C with wavelength as the parameter. Solid lines are measured data and dashed lines are the calculated values using numbers from Table I in free-carrier absorption theory: (a) *s* polarized; (b) *p* polarized.

(1)–(4)] with the parameters listed in Table I. The results are plotted as dashed lines in Fig. 2. This calculation accurately predicts the data over the entire wavelength and polar angular range. As noted earlier, there is no azimuthal angular dependence.

B. Gratings and microcavities: $\phi=90°$; *p* polarization

The differences between the *p*-polarized emittance from the shallow gratings (H approximately 1 μm) and the deeper gratings are so striking that they are discussed here as separate topics. The behavior of the deeper gratings and the microcavities is discussed in Sec. III B 2. The observed emittance maxima in the shallow gratings appear to be reasonably interpreted by the Wood's singularity model. There was no indication of structure in any of the PDSE measurements involving "hexagonal" microcavities of the type shown in Fig. 2(a) of I. As a result, only data from "wedge"-shaped microcavities [see Fig. 2(b) in I] are discussed in this paper.

1. Shallow gratings

The *p*-polarized PDSE data at $\phi=90°$ for $H=0.7$ and 1.5 μm are shown in Figs. 3(a) and 3(b). They are similar to the smooth silicon data, except for emittance maxima at θ_{max} in the $\lambda\geq5$ μm data. There are no discernible maxima in the $\lambda=3$ and 5 μm data. For $\lambda\geq7$ μm, the maxima in the PDSE show an interesting dependence. The maximum at $\lambda=7$ μm appears to split and the θ_{max} diverge as λ increases. This splitting behavior is independent of H and is remarkably similar to the Wood's singularity discussed in Sec. I. The Wood's singularity is due to a coupling of the electromagnetic wave to a surface plasmon. While the inverse process of emission is expected, it had not been observed before.

The emission process for a surface plasmon involves the coupling of the radiating wave vector k to the surface plasmon k_{SP}, with the grating effective wave vector, $2\pi/\Lambda$, as indicated in Eq. (7). Using values from Table I in Eq. 3(a), then $-10\geq\epsilon_1\geq-30$ for $\lambda\geq7$ μm. Consequently, Eq. (7) can be approximated as

TABLE I. Fitting parameters for the FCA model.

Effective mass obtained from Fig. 2	Effective mass obtained from the literature
$m^*(N=(1.2-1.6)\times10^{20}\ cm^{-3})=0.2m_0$	Low Doping: $m^*_{opt}(25\,°C)=0.26m_0$[a] $N=1.6\times10^{20}\ cm^{-3}$: $m_n^*(25\,°C)=0.36m_0$[b] $N=1.0\times10^{20}\ cm^{-3}$: $m_n^*(25\,°C)=0.30m_0$[c]
Relaxation time obtained from Fig. 2	Relaxation time obtained from the literature
$N=(1.2-1.6)\times10^{20}\ cm^{-3}$: $\tau(300\,°C)=7$ fsec	$N=0.85\times10^{20}\ cm^{-3}$: $\tau(800\,°C)=3.9$ fsec[d]
$N=(1.2-1.6)\times10^{20}\ cm^{-3}$: $\tau(400\,°C)=5$ fsec	$N=1.6\times10^{20}\ cm^{-3}$: $\tau(25\,°C)=9.0$ fsec[b]
	$N=1.6\times10^{20}\ cm^{-3}$: $\tau(25\,°C)=10.6$ fsec[d]
$N=0.85\times10^{20}\ cm^3$: Conductivity $\tau_c(800\,°C)=3.9$ fsec[d]	

[a] *Physics of Group IV Elements and III-V Compounds,* in Vol. 17a of *Landelt-Börnstein, Numerical Data and Functional Relationships in Science and Technology,* edited by O. Madelung (Springer-Verlag, New York, 1982), pp. 45, 70, 378.
[b] E. Barta, Infrared Phys. **17**, 111 (1979).
[c] A. Slaoui and P. Siffert, Phys. Status Solidi A **89**, 617 (1985).
[d] Reference 19.

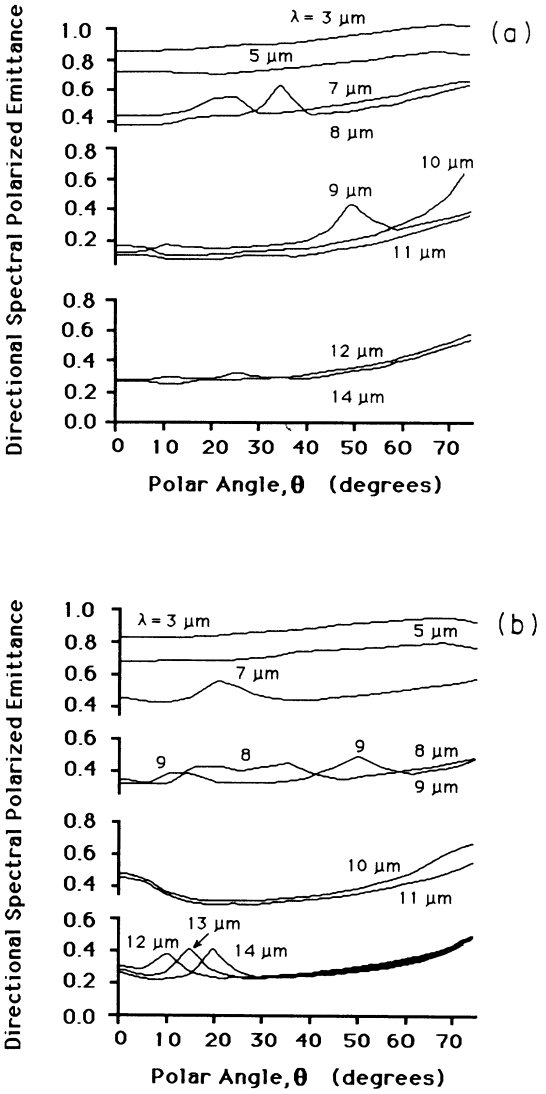

FIG. 3. p-polarized directional spectral emittance of 1.6×10^{20} cm^{-3} phosphorus-doped silicon microgrooves, with wavelength as the parameter, at $T=400$ °C, $\phi=90°$, $\Lambda=10$ μm: (a) $H=0.7$ μm, $W=6.3$ μm; (b) $H=1.5$ μm, $W=7.3$ μm.

$$\sin\theta_{\max}\approx 1-\frac{m\lambda}{\Lambda}\ . \tag{9}$$

Values for $\theta_{\max}$ were calculated for $7\ \mu\text{m}\le\lambda\le 14\ \mu$m and are listed in Table II along with the observed values for $H=0.7$ and 1.5 μm. $\theta_{\max}$ is independent of H, as predicted by Eq. (12). The agreement is excellent considering that the polar angular resolution is 0.9° and the increments are 5°. It is interesting to note that the magnitude of the emitted radiation is significantly larger for the $H=1.5$ μm structure for the longer wavelengths. The cause of this difference is not known at this time. (See *Note added in proof.)*

2. *Deep gratings*

The $\phi=90°$ PDSE data from deep microgrooves also show structure, but generally only at the longer wavelengths, see Fig. 4. Some structure is seen at shorter wavelengths and peaks are observed at polar angles corresponding to the first-order Wood's singularity at $\lambda=12,13,14$ μm. However, there are virtually no maxima for the larger values of Λ, i.e., 18 and 22 μm. Some indication of Wood's singularities were observed for $\Lambda=10$ μm and $H=3$, 7, and 14 μm. The data for the wedge-shaped microcavities show very weak maxima, and then only for the larger wavelengths.

C. Gratings and microcavities: $\phi=90°$; *s* polarization

For $H\le 3$ μm, the PDSE data are indistinguishable from the smooth surface data. A variation suggestive of a Wood's singularity mechanism is observed for the larger values of λ, see Fig. 5(a). In general, broad maxima were observed for $\lambda<W$ at roughly $\theta\approx 40\pm 15°$. Note that there is a maximum for $\lambda\le 14$ μm in Fig. 5(b), whereas this is seen only for $\lambda\le 7$ μm in Fig. 5(a). The trends suggest that the maxima move to smaller $\theta_{\max}$ as the wavelength increases. This behavior is well illustrated in Fig. 5 which is typical of the rest of the s-polarized PDSE data at $\phi=90°$. The fact that these maxima are only observed when $\lambda<W$ coincides with the cut-off wavelength behavior of the TE_{02} and TM_{02} modes in a waveguide of these dimensions. Theories of diffraction

TABLE II. Measured and calculated $\theta_{\max}$ for p-polarized emission, $\phi=90°$. The dashes mean not observed.

Wavelength (μm)	Order (m)	$\theta_{\max}^{\text{predicted}}$ (deg)	$\theta_{\max}^{\text{measured}}$ (deg)		
			$H=0.7$ μm	$H=1.5$ μm	$H=3.0$ μm
7	1	17	–	20	–
	2	23	23	–	–
8	1	11	15	18	–
	2	37	35	35	–
9	1	6	10	10	–
10	1	0	0	5	–
11	1	6	0	5	–
12	1	11	10	11	10
13	1	17	18	15	12
14	1	23	25	20	18

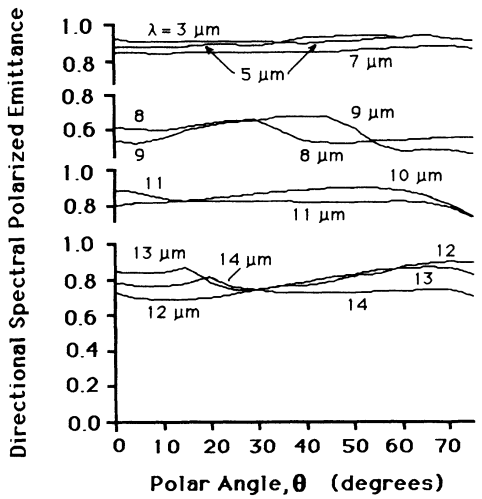

FIG. 4. p-polarized directional spectral emittance of 1.6×10^{20} cm^{-3} phosphorus-doped silicon microgrooves, with wavelength as the parameter, at $T=400$ °C, $\phi=90°$, $\Lambda=10$ μm, $H=53$ μm, and $W=7.3$ μm.

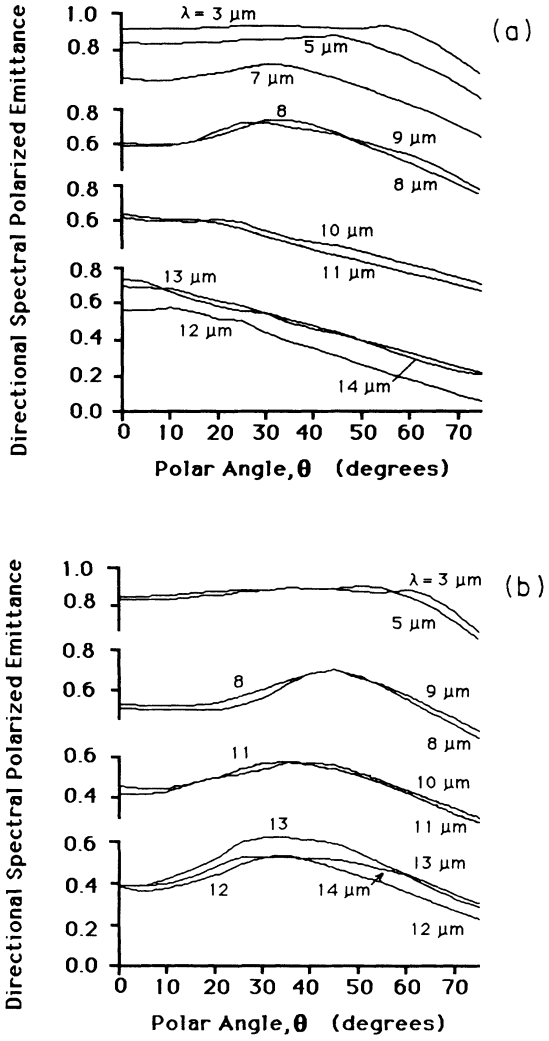

FIG. 5. s-polarized directional spectral emittance of 1.6×10^{20} cm^{-3} phosphorus-doped silicon microgrooves, with wavelength as the parameter, at $T=400$ °C, $\phi=90°$: (a) $\Lambda=10$ μm, $H=53$ μm, $W=7.3$ μm; (b) $\Lambda=22$ μm, $H=42$ μm, $W=14$ μm.

and the emission from a waveguide have been examined.[3] In both cases, θ_{max} should be proportional to λ. This is clearly not the case with these data. The data for wedged-shaped microcavities are quite similar to the grating data of corresponding Λ. Again, when $\lambda > W$, the amplitude of the emittance peak is reduced significantly.

D. Gratings: $\phi=0°$; s polarization

For $\phi=0°$, the radiation is emitted perpendicular to the grating vector of the MC surface (see Fig. 1). This plane is orthogonal to the plane of incidence considered in diffraction ($\phi=90°$). This orientation corresponds to the "conical diffraction" mode in eschelette gratings.[22] It is appropriate at this point to note that radiation absorption processes occurring in the lamellar structures treated here are dominated by the modal structure of the cavities. It has been pointed out by several authors that calculations of the modal behavior of gratings with finite conductivities are far from simple.[23,24] Therefore, it was not surprising that no previous studies were found on emittance or absorptance for $\phi=0°$.

A larger number of measurements were conducted for $\phi=0°$. Again, for clarity, only those results which illustrate the principal features of these measurements are given. All the $e(\lambda,\theta,0°,s,400\,°C)$ data for deep slots with $10\ \mu m \le \Lambda \le 22\ \mu m$ show periodic variations with θ at the longer wavelengths which are independent of Λ, even though Λ varies by a factor of 2.2. In Fig. 6(a), $e(14\ \mu m,\theta,0°,s,400\,°C)$ is shown for $H\approx47$ μm with Λ as the parameter. The lack of a Λ dependence in these maxima is quite striking. The simplest interpretation of these results is that the maxima are due to coupling between the **k** vector of the emitted radiation and the Planckian modes shown schematically in Fig. 6(b). The measured values of θ_{max} for the complete $e(\lambda,\theta,0°,s,400\,°C)$, $H\approx47$ μm, data set is listed in Table III. Interestingly enough, the emission maxima for the larger values of Λ are only seen at larger θ.

To account for this behavior, the wave vector of the emitted s-polarized radiation must be coupled to the quantized vertical Planckian modes. In this azimuth, the s-polarized field is perpendicular to the microgrooves corresponding to the E_y electric field component of the TM waveguide mode. See Fig. 6(c) for the coordinate system. When $\phi=0°$, the plane of observation remains in the z-x plane as θ is varied. Since the Planckian modes are present in the z direction, the wave vector for the E_y component of the electric field is quantized in the z direction by the geometry. A continuum of modes exists in the x direction. This is represented in k space as sheets with mode numbers a distance $\pm\pi/H$ apart along k_z. For coupling to take place, the z component of the wave vector of the emitted radiation must equal k_z in the direction of observation, i.e.,

$$k_{max}\cos\theta_{max}=k \ , \tag{10}$$

but since $k_z=\pm m\pi/H$ and $k_{max}=2\pi/\lambda_{max}$, then

$$m\lambda_{max}=2H\cos\theta_{max} \ , \tag{11}$$

where m is the integer order 2 through 5. In Fig. 7 the $\cos\theta_{max}$ of the PDSE for $\phi=0°$ are plotted against λ_{max}. A linear regression with a zero intercept provided a satisfactory fit to the data found. Only the $\Lambda=10$ and 14 μm maxima are plotted but the other data agreed equally well. Using the slope of $m/2H$ from Eq. (2), a value of $H=36\pm4$ μm was obtained from the average slope in Fig. 7. This is in reasonable agreement with the average calculated depth of 40 ± 5 μm from the slope of $k_{max}(m)$ for $\theta=0°$ found in I and the average optically measured depth of 47 ± 8 μm. It is not clear why the coupling occurs only for the s-polarized emission which corresponds to a TM waveguide mode. Furthermore, there is

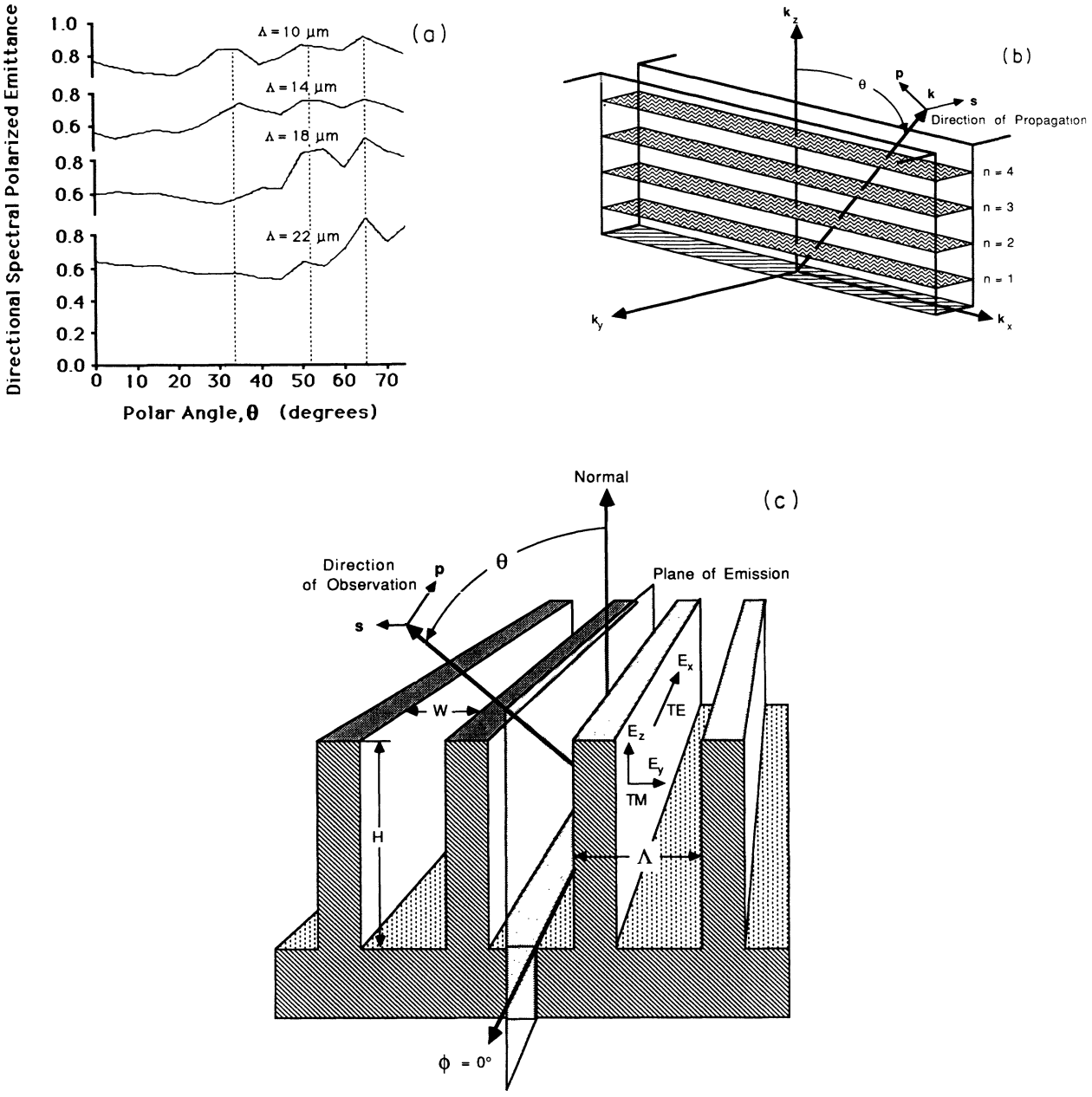

FIG. 6. (a) s-polarized directional spectral emittance of 1.6×10^{20} cm^{-3} phosphorus-doped silicon microgrooves at $\lambda=14$ μm with Λ as the parameter at $T=400$ °C, $\phi=0°$, $H\approx47$ μm. The dashed vertical lines emphasize the alignment of the PDSE maxima for the four different Λ's. (b) Illustration of the quantized propagation vector ($n=1-4$) for the s-polarized emission ($\phi=0°$). (c) Schematic drawing of the $\phi=0°$ plane of emission in a deep grating. Also illustrated are the TE and TM electric fields in relationship to the s- and p-polarization vectors. θ is the polar angle with respect to the normal.

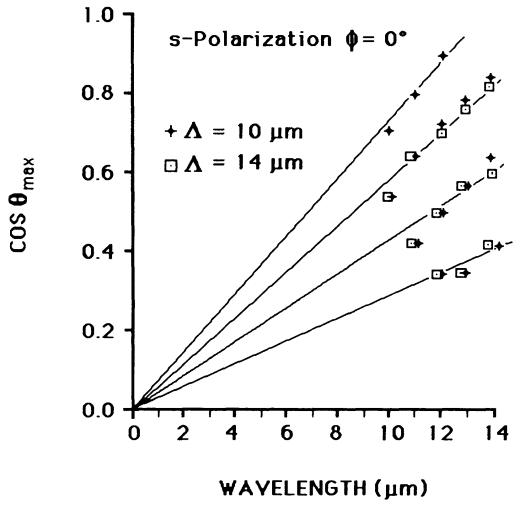

FIG. 7. $\cos\theta_{max}(\lambda_{max})$ of s-polarized directional spectral emittance of 1.6×10^{20} cm^{-3} phosphorus-doped silicon microgrooves, $H\approx47$ μm at $\phi=0°$ for $\Lambda=10$ and 14 μm.

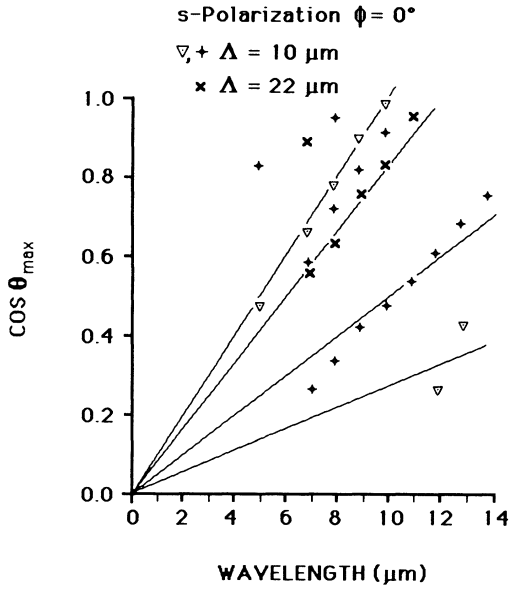

FIG. 8. $\cos\theta_{max}(\lambda_{max})$ for s-polarized directional spectral emittance of 1.6×10^{20} cm^{-3} phosphorus-doped silicon microgrooves at $\phi=0°$, $H=13$ μm ($\times$), $\Lambda=22$ μm; $H=7$ μm (+), $\Lambda=10$ μm; $H=14$ μm (∇), $\Lambda=10$ μm.

no simple explanation for the maxima appearing only for $\theta>35°$.

Multiple peaks are also present in gratings with shallower slots, 1.5 μm $\leq H\leq 14$ μm. In Fig. 8, $\cos\theta_{max}$ is plotted against λ_{max} for two gratings, $H=7$ μm, $\Lambda=10$ μm and $H=13$ μm, $\Lambda=22$ μm. 12 and 5.3 μm are obtained for H from the slopes of these lines, in reasonable agreement with the optically measured values of 13 and 7 μm, respectively.

There are peaks in the emittance of shallower gratings with $H<3$ μm, as seen in Figs. 9(a). The peak moves to smaller θ as λ increases, in general agreement with the Planckian mode, standing-wave model. There is almost no dependence on H in these shallow gratings. This behavior may arise from the triangular trough at the bottom of the grating slot. The depth of the apex of the trough is much less dependent on H at these small values of H. The resolution of this behavior requires further experimental study. The data for the wedge-shaped microcavities showed little structure.

E. Gratings and cavities: $\phi=0°$; p polarization

The PDSE of the shallow gratings, $H<1.5$ μm, is identical to that of smooth silicon. When $H>3$ μm, other features are observed, see Fig. 10(a), for $W=10$ μm,

TABLE III. θ_{max} for s-polarized emittance at $\phi=0°$, $H=47$ μm. The dashes mean not observed.

Wavelength (μm)	Order (m)	$\theta_{max}^{predicted}$ (deg)	$\theta_{max}^{measured}$ (deg)			
			$\Lambda=10$ μm	$\Lambda=14$ μm	$\Lambda=18$ μm	$\Lambda=22$ μm
14	4	38	32	35	–	–
	3	54	50	53	52	50
	2	67	65	65	65	65
13	4	43	39	40	–	–
	3	57	55	55	55	55
	2	68	70	70	70	65
12	5	33	26	–	–	–
	4	48	44	45	–	–
	3	60	60	60	60	60
	2	70	70	70	70	70
11	5	40	37	–	–	–
	4	52	50	50	–	–
	3	62	65	65	–	–
	6	33	30	–	–	–
10	5	46	45	–	–	–
	4	56	57	57	–	–

$H=7$ μm. These data display a broad maximum, where θ_{max} decreases with increasing λ. However, the position of the peak is not a simple function of H and Λ. In Fig. 10(b), it is seen that $\cos\theta_{max}$ varies linearly with λ_{max}. By employing Eq. (11), dimensions may be calculated from the slopes which are determined to be 6.5 μm for $\Lambda=10$ μm, 8.5 μm for $\Lambda=14$ μm, 11.7 μm for $\Lambda=18$ μm, and 14.3 μm for $\Lambda=22$ μm. These values are in remarkable agreement with the corresponding widths of the slots in the gratings, i.e., 7.3 μm for $\Lambda=10$ μm, 8.4 μm for $\Lambda=14$ μm, 12.6 μm for $\Lambda=18$ μm, and 14.0 μm for $\Lambda=22$ μm. This again suggests that standing-wave Planckian modes similar to those responsible for the maxima in the s-polarized $\phi=0°$ PDSE are responsible for the observed maxima. The critical difference here is that the characteristic dimension is the width of the grooves instead of the depth.

If the grating slots are viewed as a waveguide, then the TE and TM waveguide modes have electric field components E_x and E_z, respectively, as shown in Fig. 6(c). These components will couple to a p-polarized electromagnetic wave at $\phi=0°$. At $\theta=0°$, the p-polarized wave is coupled to the E_x component and at $\theta=90°$, to the E_z component. At intermediate angles there is a partial coupling. The k vectors of both E_z and E_x are quantized in y and, in addition, the k vector of E_x is quantized in z. The results on the p polarized, $\phi=0°$ PDSE strongly suggests that there is a first-order ($n=1$) quantized wave vector in the k_y direction. However, it is not clear why the k_z quantization is not observed.

The remainder of the microgrooves studied show similar maxima. A peak is observed in the PDSE in the same

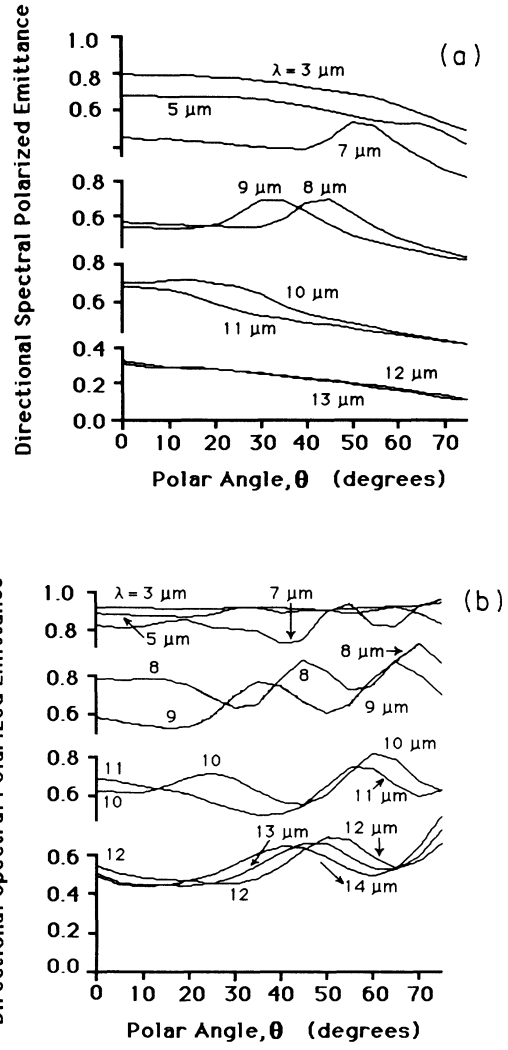

FIG. 9. s-polarized directional spectral emittance of 1.6×10^{20} cm^{-3} phosphorus-doped silicon shallow microgrooves, with wavelength as the parameter, at $T=400$ °C, $\phi=0°$, $\Lambda=10$ μm. (a) $H=1.5$ μm, $W=7.3$ μm; (b) $H=14$ μm, $W=8.4$ μm.

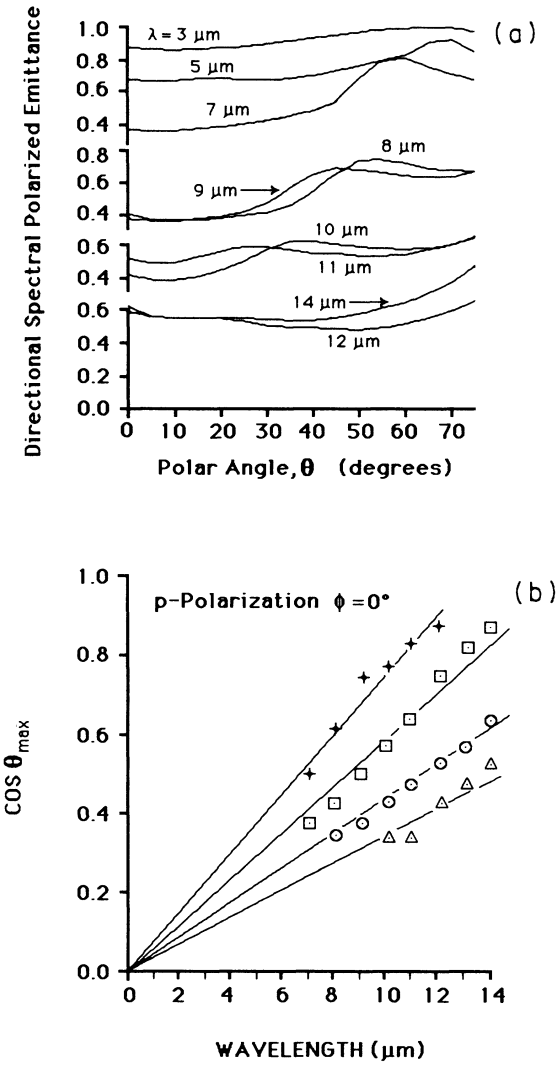

FIG. 10. (a) p-polarized directional spectral emittance of 1.6×10^{20} cm^{-3} phosphorus-doped silicon microgrooves, with wavelength as the parameter, at $T=400$ °C, $\phi=0°$, $\Lambda=10$ μm, $H=7$ μm, $W=7.3$ μm. (b) $\cos\theta_{max}(\lambda_{max})$ of p-polarized directional spectral emittance of 1.6×10^{20} cm^{-3} phosphorus-doped silicon microgrooves at $\phi=0°$, $H\approx47$ μm, $\Lambda=22$ μm (△), 18 μm (⊙), 14 μm (□), and 10 μm (+).

polar angle range as for the deep grooves. While θ_{max} decreases in an approximately linear fashion with increasing λ_{max}, the intercept is not always zero. Here, too, no simple explanation is apparent for this behavior. As was the situation with the other PDSE measurements cavities, the data for this azimuth and polarization show little structure.

IV. CONCLUSIONS

As pointed out in I, there are essentially no direct theoretical results that have a bearing on the experimental results obtained. Such work as has been done suggests the absence of absorption processes that are clearly observed in the normal direction. The observation of not only first-order Wood's singularities in I but also the presence of second-order singularities in the *p*-polarized directional spectral emittance confirms that this measurement technique is a powerful tool for exploring electromagnetic resonant processes occurring in microstructures. In reviewing the literature, it has been clear that there are significant disagreements between the resonant processes we observe and the theoretical calculations performed to date, especially on *s*-polarized, $\phi=0°$ and 90° polar emission. Even more striking is the observed resonance on the *p*-polarized, $\phi=0°$ observations. We conclude that there have been no discussions of resonance in the so-called conical diffraction case that would relate the electromagnetic modal structure to these observations.

The extraordinary diversity of structure in the emittance data observed in this study and the preceding paper demonstrate that small microstructures in modestly conducting materials like doped silicon gives rise to well-defined, finite density, radiating electromagnetic modes on their surfaces. Consequently, these results support the discussion of Baltes and co-workers that the emission characteristics of small radiators are profoundly different from macroscopic blackbodies because of the finite density of allowed electromagnetic modes.[24,25] Since the thermal energy populates all existing modes with the thermodynamically available electromagnetic energy, PDSE measurements are particularly well suited for studying the varied characteristics of these modes, including their geometric dependence, the interaction between the electromagnetic field and the finite conducting walls of the microstructures, and the energy distribution of the modes. It has been suggested in some private discussions that reflectance measurements are equally suited for this type of measurement. While the same information may be extracted because of Kirchoff's law, the presence of diffracted orders tends to complicate the observations. It is for this reason that we conclude that emittance is a versatile tool for studying the electromagnetic characteristics of microstructured elements. This contrasts with earlier measurements in which the directional spectral emission behavior was largely an adjunct to conventional optical measurements.[26]

All the *s*-PDSE at $\phi=90°$ have a broad maxima in the general range of θ near 40°. This angular value coincides with the cut-off wavelength of the TE_{02} and TM_{02} modes of a waveguide with the same dimensions. However, the emission does not have the wavelength dependence predicted by waveguide theory. This persistent feature has not been related to any standard electromagnetic theory for cavity antennae. The understanding of these resonances will require further developments in theory.

Radiative processes have always been a very important consideration in heat-transfer studies. Conventionally, only total directional and spectral emittances have been available for modeling radiative transfer, and that only for a very few materials and surface conditions. The high degree of anisotropy observed in the emission from the grating MC structure point out the limitations of past conventional methodologies in studying randomly roughened surfaces. These measurements clearly demonstrate that resonances occur in both *s*- and *p*-polarized emission from gratings.

To summarize the results on the PDSE of lamellar gratings: the resonances in the *s* polarization at $\phi=0°$ demonstrate the coupling of the quantized k_z wave vector to a radiating wave; the *p*-polarized emission at $\phi=0°$ is coupled to the quantized k_y wave vector and not to k_z. A better description for this coupling process is needed. Because the standing-wave modes couple to the radiating modes so well (high emittance at the resonant wavelength), the microgrooves are efficient antennae. From the *p*-polarized PDSE at $\phi=90°$, the first two orders of the Wood's anomaly are readily observed on shallow gratings but become masked by the Planckian mode resonant peaks in the deeper grooves. While the *s*-polarized spectral emittance at $\phi=90°$ and normal incidence shows pronounced resonances for deep gratings, the polar angular dependence of the corresponding PSDE requires further study. Finally, the parameters obtained by fitting the free-carrier absorption theory to the directional emissivity measurements on smooth, heavily doped silicon is in excellent agreement with other values in the literature.

Note added in proof. Neviere presents the results of a calculation that demonstrates that the type of variation illustrated in Fig. 3 is due to variations in the poles and zeros of the emitted intensity [M. Neviere, in *Electromagnetic Theory of Gratings,* edited by R. Petit (Springer-Verlag, Berlin, 1980), p. 136].

ACKNOWLEDGMENTS

The authors wish to acknowledge the following: Judson Infrared, Montgomeryville, PA, for their contribution of a the HgCdTe infrared detector; Dr. A. Ipri of the RCA Sarnoff Laboratory for supplying the photomasks; Dr. Anatoly Feygenson of the AT&T Bell Laboratories, Reading, PA, for the spreading resistance measurements; the partial support of the EEMS program of the National Science Foundation under Grant No. ECS-84-12241 (P.H. and J.N.Z.); support from the National Science Foundation Grant No. CBT 84-18517 (B.G.); useful discussions with Professor H. Baltes and Professor A. Maradudin (J.N.Z. and P.J.H.).

*Now at SRI International, Menlo Park, CA 94025.
[1]P. J. Hesketh, J. N. Zemel, and B. Gebhart, Nature (London) **324**, 549 (1986).
[2]P. J. Hesketh, J. N. Zemel, and B. Gebhart, preceding paper, Phys. Rev. B **37**, 10 795 (1988).
[3]M. Born and E. Wolf, *Principles of Optics,* 6th ed. (Pergamon, New York, 1984), p. 401.
[4]K. Seeger, *Semiconductor Physics* (Springer-Verlag, New York, 1973).
[5]R. Sieger and J. R. Howell, *Thermal Radiation Heat Transfer,* 2nd ed. (McGraw-Hill, New York, 1981).
[6]J. A. Stratton, *Electromagnetic Theory* (McGraw-Hill, New York, 1941).
[7]C. H. Liebert, in *Progress in Astronautics and Aeronautics: Thermophysics of Spacecraft and Planetary Bodies,* edited by G. B. Heller (Academic, New York, 1967), Vol. 20, p. 17.
[8]R. W. Wood, Philos. Mag. **4**, 396 (1902).
[9]C. H. Palmer, J. Opt. Soc. Am. **46**, 50 (1956).
[10]A. Hessel and A. A. Oliner, App. Opt. **4**, 1275 (1965).
[11]Y.-Y. Teng and E. A. Stern, Phys. Rev. Lett. **19**, 511 (1967).
[12]D. Maystre, in *Electromagnetic Surface Modes,* edited by A. D. Boardman (Wiley, New York, 1982), p. 661.
[13]A. Wirgin and R. Deleuil, J. Opt. Soc. Am. **59**, 1348 (1969).
[14]C. H. Palmer, F. C. Evering, Jr., and F. M. Nelson, Appl. Opt. **4**, 1271 (1965).
[15]J. E. Stewart and W. S. Gallaway, Appl. Opt. **1**, 421 (1962).
[16]M. C. Hutley and D. Maystre, Opt. Commun. **19**, 43 (1976).
[17]E. G. Loewen and M. Neviere, Appl. Opt. **16**, 3009 (1977).
[18]M. C. Hutley, J. F. Verrill, and R. C. McPhedran, Opt. Commun. **11**, 207 (1974).
[19]R. E. Rolling, in *Progress in Astronautics and Aeronautics: Thermophysics of Spacecraft and Planetary Bodies,* edited by G. B. Heller (Academic, New York, 1967), Vol. 20, p. 91.
[20]P. Demont, M. Hvetz-Aubert, and H. Trann'guyen, Int. J. Thermophys. **3**, 335 (1982).
[21]P. J. Hesketh, B. Gebhart, and J. N. Zemel, J. Heat Transfer (to be published).
[22]R. Petit, in *Electromagnetic Theory of Gratings,* edited by R. Petit (Springer-Verlag, Berlin, 1980), p. 31.
[23]R. C. McPhedran, G. H. Derrick, and L. C. Botten, in *Electromagnetic Theory of Gratings,* edited by R. Petit (Springer-Verlag, Berlin, 1980), p. 228.
[24]H. P. Baltes and E. R. Hilf, *Spectra of Finite Systems* (Bibliographische Institute-Wissenschaftsverlag, Zurich, 1976). This book provides an excellent overview of the current theoretical state of the Weyl problem of calculating the density of states in finite systems and demonstrates the discrete character of the density of allowed states in such finite systems.
[25]H. P. Baltes, Infrared Phys. **16**, 1 (1976).
[26]D. L. Stierwalt, Appl. Opt. **5**, 1911 (1966).

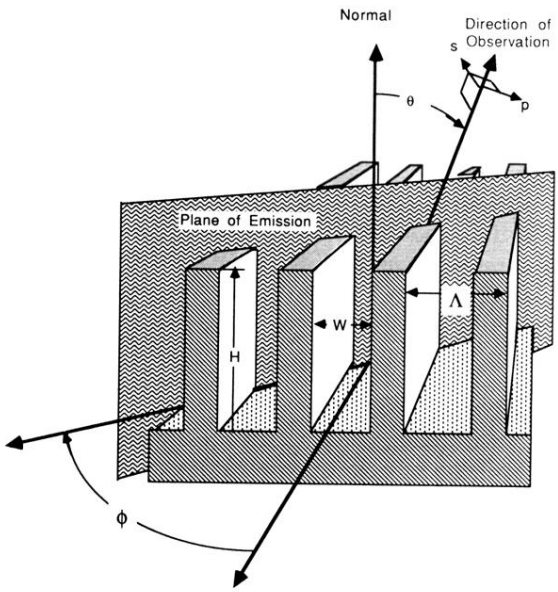

FIG. 1. Coordinate system for the polarized, directional, spectral emittance. Λ is the grating propagation vector, H is the depth of the grating slot, W is the width of the slot, θ is the polar angle measured relative to the normal to the microconfigured surface, and ϕ is the azimuthal angle. The p polarization lies in the plane of emission and the s polarization is perpendicular to that plane. Not shown is the length of the slots, L.

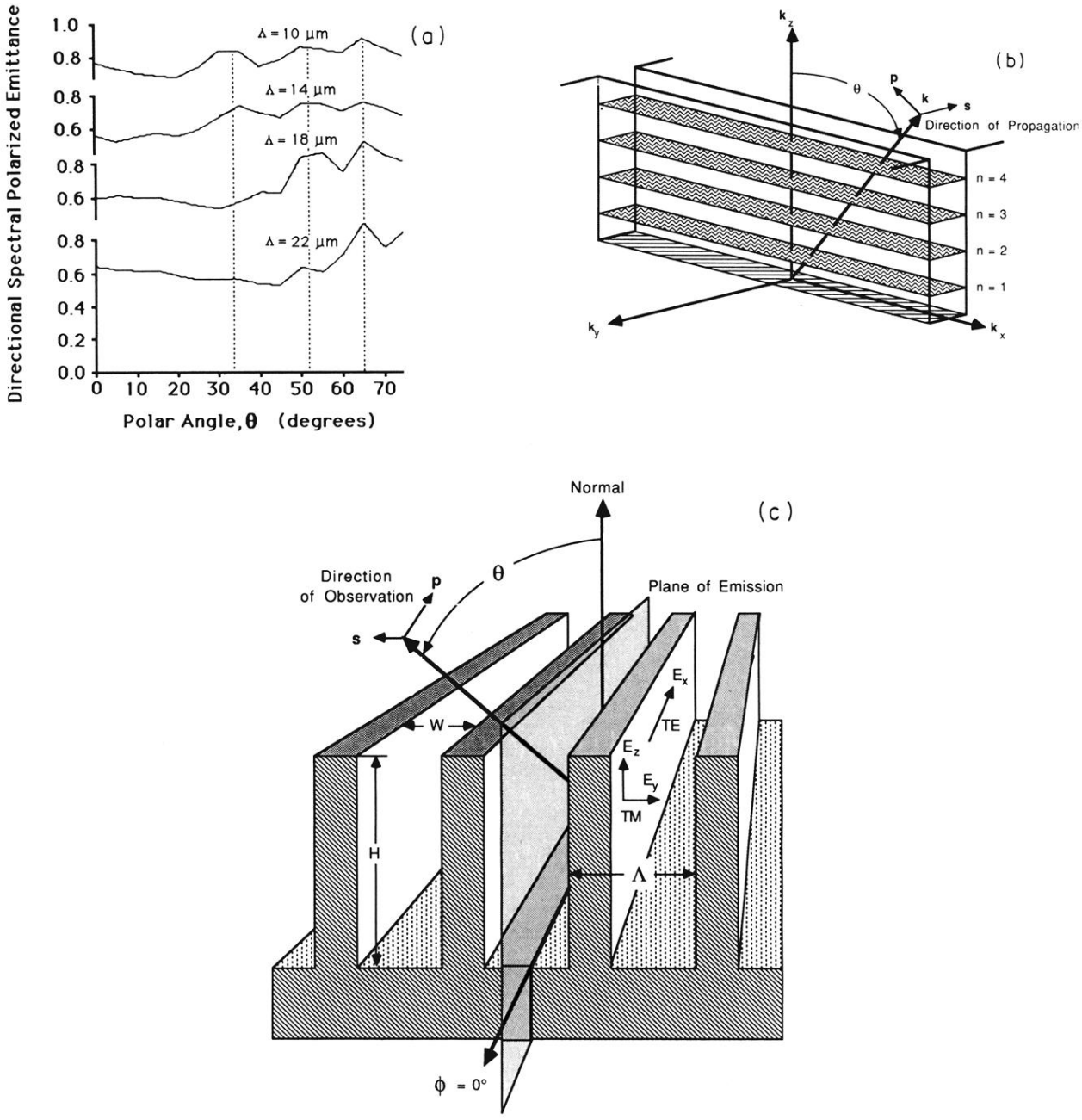

FIG. 6. (a) *s*-polarized directional spectral emittance of 1.6×10^{20} cm^{-3} phosphorus-doped silicon microgrooves at $\lambda=14$ μm with Λ as the parameter at $T=400$ °C, $\phi=0°$, $H\approx47$ μm. The dashed vertical lines emphasize the alignment of the PDSE maxima for the four different Λ's. (b) Illustration of the quantized propagation vector ($n=1$–4) for the *s*-polarized emission ($\phi=0°$). (c) Schematic drawing of the $\phi=0°$ plane of emission in a deep grating. Also illustrated are the TE and TM electric fields in relationship to the *s*- and *p*-polarization vectors. θ is the polar angle with respect to the normal.